

# Crystallization and morphology of poly(aryl-ether-ether-ketone)

Satish Kumar and David P. Anderson

University of Dayton Research Institute, Dayton, OH 45469, USA

and W. Wade Adams

Materials Laboratory, Air Force Wright Aeronautical Laboratories, Wright Patterson AFB, OH 45433, USA

(Received 29 March 1985; revised 17 October 1985)

The morphology of poly(aryl-ether-ether-ketone) (PEEK) has been studied using optical microscopy (at room temperature and at elevated temperatures), small-angle light scattering ( $H_v$  and  $V_v$ ), transmission electron microscopy (bright field, dark field, and selected area electron diffraction), and wide and small-angle X-ray scattering. As expected, density of nucleation and hence spherulite size depends on melt temperature. Higher melt temperatures give rise to low nucleation density and hence large spherulites. The spherulite growth rate is independent of melt temperature and depends on crystallization temperature. The sign of the spherulite birefringence was determined between room temperature and 320°C by polarizing microscopy and at room temperature by  $V_v$  light scattering. In this temperature range the spherulites were negatively birefringent. From selected area electron diffraction, the crystal unit cell  $b$ -axis is found to align along the radius of the spherulite. The crystallographic (110) plane, which makes an angle of 52.7 degrees with the radial  $b$ -axis, appears to be the preferred growth plane. Chain polarizability was also calculated using refined atomic coordinates and the bond polarizabilities. PEEK crystals were more stable in the electron beam, by about an order of magnitude, than polyethylene.

(Keywords: poly(aryl-ether-ether-ketone); spherulite; birefringence; SAXS; WAXS; SALS; nucleation density; transmission electron microscopy)

## INTRODUCTION

Poly(aryl-ether-ether-ketone) (PEEK), whose repeat unit is shown in *Figure 1a*, crystallizes into an orthorhombic unit cell structure<sup>1-3</sup>. The synthesis of this family of polymers is described by Attwood *et al.*<sup>4</sup>. Crystallization behaviour and spherulitic growth have been studied by Blundell and Osborn<sup>5</sup>, and PEEK was shown to behave much in the same way as poly(ethylene terephthalate). The morphology and solution properties of PEEK have been the subject of recent studies<sup>6-8</sup>.

The orthorhombic unit cell of PEEK has values of  $a$ ,  $b$  and  $c$  which are reported to be in the range of 7.75–7.78 Å, 5.89–5.92 Å and 9.88–10.06 Å respectively. The unit cell contains two chains each with two-thirds of the repeat unit. However, a unit cell with two repeat units has recently been considered<sup>9</sup>. The crystal structure of PEEK is similar to the reported<sup>10</sup> crystal structure of poly(*p*-phenylene oxide), and the ether and carbonyl units are considered to be crystallographically equivalent<sup>3</sup>. The crystal structure is shown in *Figure 1b*.

PEEK is a candidate as a thermoplastic to be used in composites<sup>11</sup>, the properties of which will depend on processing history and morphology. Therefore the understanding of morphology and its dependence on processing parameters is important. We have studied the crystallization behaviour of PEEK from the melt in a polarizing microscope. The morphology of PEEK spherulites has been studied using light and X-ray scattering, optical microscopy, as well as transmission electron microscopy (dark field, bright field, and selected area electron diffraction). The results of these investigations are reported in this paper.

## EXPERIMENTAL

Studies reported in this paper were conducted on commercially available PEEK received from Imperial Chemical Industries.

Crystallization studies were done in a metallurgical hot stage on a Leitz optical microscope. A very small amount of PEEK resin (few milligrams) is sandwiched between two circular glass plates of about half a centimeter diameter. The hot stage is then heated to the desired melt temperature (between 380°C and 420°C), above the melting point of PEEK, which is reported to be in the range of 335°C to 350°C. After five minutes at the melt temperature the hot stage is set to the crystallization temperature (300 or 320°C) and the hot stage containing the specimen reaches this temperature in approximately 30 s. Spherulite growth was recorded at the crystallization temperature as a function of time, using crossed polars, on Kodak VR1000 35 mm film.

Wide-angle X-ray scattering (WAXS), transmission electron microscopy (TEM), and small-angle X-ray scattering (SAXS) were performed on the samples prepared in the following way. A mould containing the resin was placed in a compression moulding press preheated to 400°C, and nominal pressure was applied. A thermocouple was in contact with the resin. In one case, five minutes after the thermocouple reached 400°C the press heaters were turned off. The specimen reached room temperature in about three hours. This specimen is referred to as slow cooled (SC). In another case, five minutes after the thermocouple reached 400°C, the mould containing the resin was removed from the hot press and kept in a second press which was at room temperature.

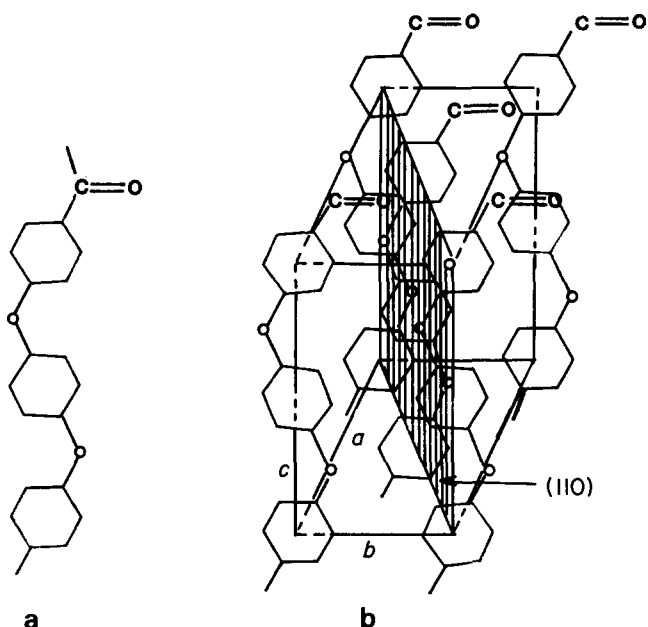


**Figure 1** (a) Repeat unit of poly(aryl-ether-ether-ketone). (b) Unit cell of PEEK (*c*-axis is shown from the centre of the first phenyl ring to the centre of the third phenyl ring)

This specimen came to room temperature in a few minutes and is referred to as fast cooled (FC). Similar samples were also made from 420°C.

WAXS was carried out using the symmetric transmission geometry on a four circle automated Picker diffractometer. Lorentz, polarization, Compton scattering, and absorption corrections were applied. Correction for instrumental line broadening for the crystal size measurement was done using crystalline hexamethylenetetramine. For TEM, thin sections were prepared by ultramicrotoming epoxy embedded blocks of PEEK at room temperature using a diamond knife. Transmission electron microscopy was done on a JEOL 100CX at 100 kV, SAXS was carried out on a modified Statton (Warhus) camera with pin-hole collimation, camera-to-film distance of 72 cm, and  $\text{CuK}\alpha$  radiation. No corrections were applied to the SAXS data.

## RESULTS AND DISCUSSION

### Nucleation and growth

Isothermal crystallization of PEEK at 320°C, from the melt at 380°C and at 420°C, is shown in *Figures 2 and 3* respectively. In *Figure 2* only the completion of spherulite growth is shown. This is because nucleation density was high in the specimens crystallized from lower melt temperatures, so that spherulites filled the volume rather quickly and spherulitic growth could not be monitored visually. However such growth can be monitored with a state of the art, automated small-angle light scattering apparatus<sup>12</sup>. *Figure 3* shows crystallization from higher melt temperature, with lower nucleation density.

Spherulitic growth rate was monitored at crystallization temperatures of 300°C and 320°C from a melt of 420°C by measuring the spherulite radii from optical micrographs taken at successive intervals. The radius can also be calculated from small-angle light scattering (Hv) using the following equation

$$4\pi(R_s/\lambda)\sin(\theta_{\max}/2) = 4.1 \quad (1)$$

where  $\theta_{\max}$  is the angle at maximum intensity,  $\lambda$  is the wavelength of light, and  $R_s$  is the radius of the spherulite. For two-dimensional spherulites<sup>13</sup> the constant in equation (1) will be 3.8 instead of 4.1. Typical Hv and Vv light scattering patterns of PEEK at room temperature are given in *Figure 4*. Spherulite sizes from optical micrographs and from SALS were identical within the limits of experimental error. Average spherulite radius, measured from optical micrographs up to the point where they start impinging on each other, has been plotted in *Figure 5* for a crystallization temperature of 320°C. The growth is linear and the average growth rates were  $0.045 \mu\text{m s}^{-1}$  at 320°C and  $0.32 \mu\text{m s}^{-1}$  at 300°C. Blundell and Osborn have reported the maximum crystallization rate to occur at 230°C, as studied from differential scanning calorimetry, with some dependence on heating rate. Qualitatively our spherulite growth data are in agreement with this observation in that we observe a higher growth rate at 300°C than at 320°C. However, quantitatively the growth rate observed by us at 300°C corresponds to that between 260°C and 270°C by Blundell and Osborn (the values of *G* in Table 3 of ref. 5), and extrapolation of their data to 300°C would give a lower growth rate than that we have observed. This may occur for several reasons: (i) differences in molecular weight, (ii) secondary crystallization which will be observed in d.s.c. but not in optical micrographs, and (iii) Blundell and Osborn calculated growth rate assuming that the peak crystallization time,  $t_c$ , corresponds to the point where the spherulites impinge. Peak crystallization time would be analogous to the crystallization time for *Figure 3c* of this paper, which is an overestimation, because the majority of the spherulites have stopped growing much earlier (*Figure 3b*).

A plot of the logarithm of nucleation density (number of spherulites per unit volume) as a function of melt temperature is given in *Figure 6*. Within the temperature range of the experiment nucleation density seems to fall off exponentially with the temperature increase (logarithm of nucleation density as a function of temperature is linear within the limits of experimental error). Observation of the change in nucleation density in PEEK, as a function of the temperature to which the melt was heated and the dwell time at the high temperature, is by no means unique and has been reported for a number of polymers<sup>14</sup>.

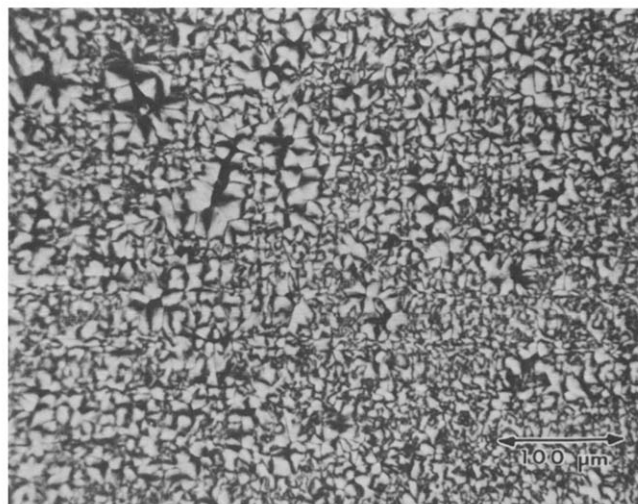


**Figure 2** PEEK spherulites between cross polars at crystallization temperature (300°C). Melt conditions—5 min at 380°C

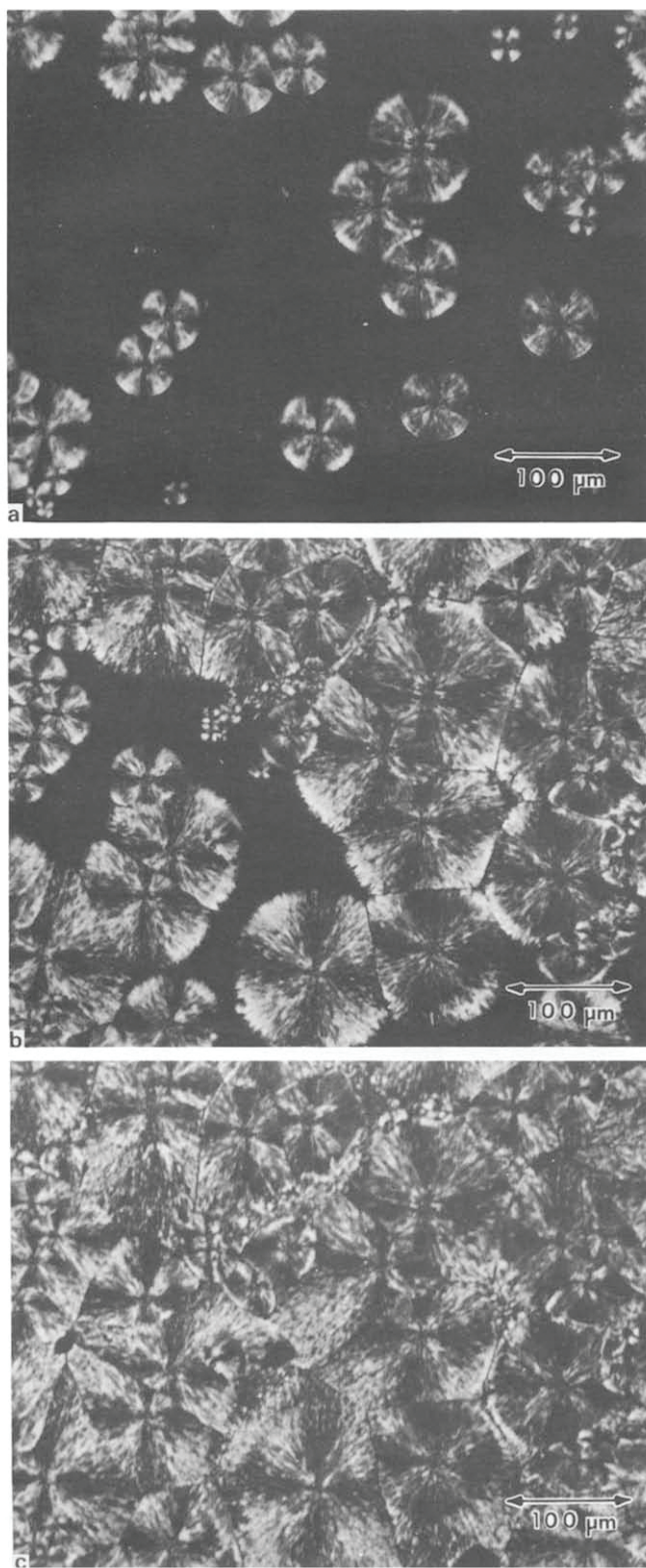


Figure 3 Growth of PEEK spherulites, melt conditions—5 min at 420°C, crystallization temperature 320°C. Photographs taken at 320°C between cross polars after (a) 8 min, (b) 16 min and (c) 24 min

Possible reasons for the change in nucleation density as a function of the melt temperature are discussed below.

(i) The melting point of PEEK has been reported to be 335°C (refs. 4 and 5) and 350°C (ref. 15). However, the thermodynamic melting temperature, at which perfect crystals of infinite size melt, has been estimated<sup>4</sup> to be 395°C. This leads to the possibility of the presence of some unmelted crystals at a temperature higher than the

normally measured melting point. Self nucleation by residual high molecular weight crystals can also possibly account for the above observation<sup>14</sup>. The degree of self nucleation (number of embryos) decreases with

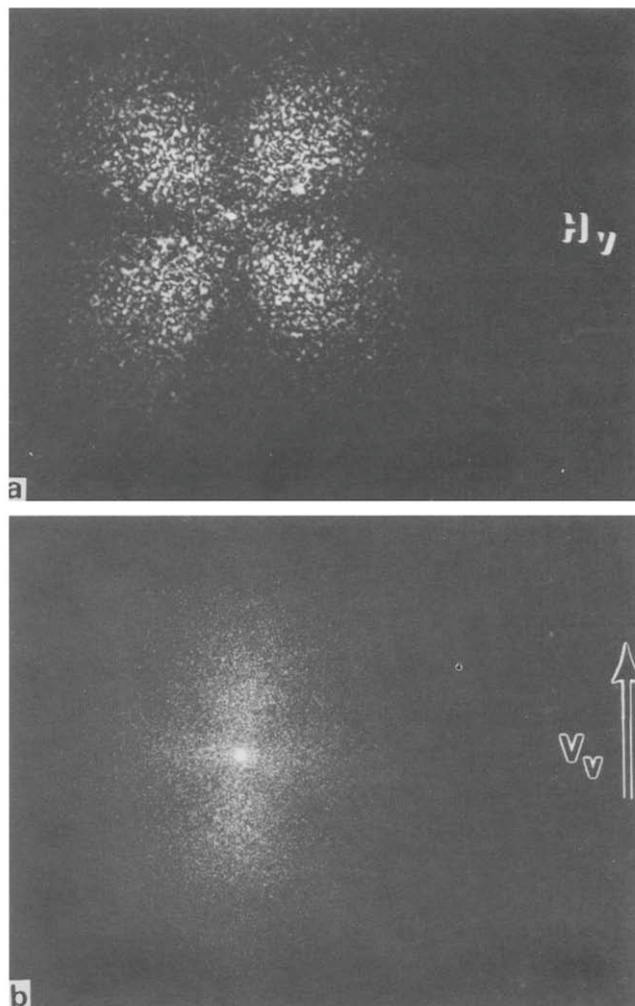


Figure 4 (a)  $H_v$ , and (b)  $V_v$  light scattering patterns of PEEK crystallized from melt at 420°C

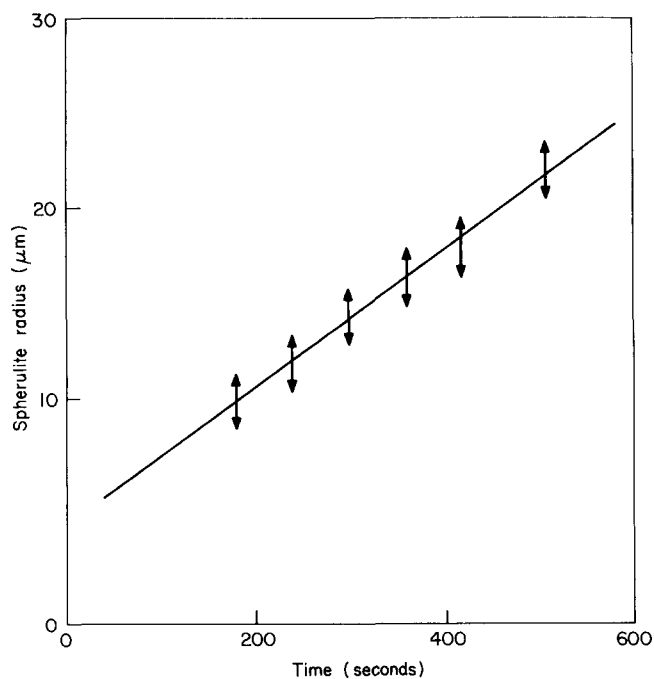


Figure 5 Linear isothermal radial growth of PEEK spherulite at 320°C

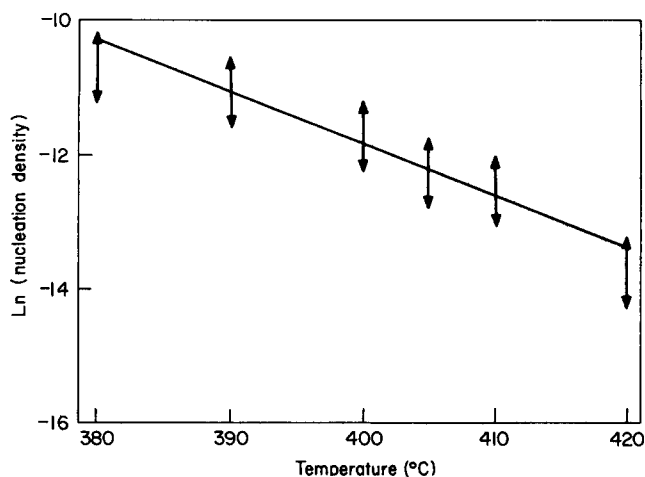


Figure 6 Plot of logarithm of nucleation density ( $\mu\text{m}^{-3}$ ) as a function of melt temperature

increasing temperature, and hence results in larger spherulite size from higher melt temperatures.

(ii) Impurities in the specimen can lead to nucleation. A decrease in nucleation density has been observed on purifying the material<sup>7</sup>. The purification was done by dissolving the material in sulphuric acid and reprecipitating it. The problem of sulphonation of PEEK during treatment in sulphuric acid also remains. In addition to the impurities which were removed in acid the possibility of the presence of some other species of the poly(aryl-ether-ketone) family (one of the species is reported<sup>4</sup> to have a melting point of 416°C) can not be excluded as a result of impurities in the starting materials used in the synthesis. Since ether and ketone units are crystallographically equivalent<sup>3</sup> certain different species of the poly(aryl-ether-ketone) family may be able to crystallize together. One nucleating crystal in one hundred billion crystals of average dimension of 100 Å, in a 50% crystalline medium, will produce an average spherulite radius of 36  $\mu\text{m}$ .

Since the melting and crystallization studies reported in this paper are done at rather high temperatures, it is only natural that the effect of these conditions on polymer degradation be considered. The large spherulite size has in fact been attributed to degradation from high melt temperatures<sup>7</sup>. Therefore the effect of air at high temperatures must be considered. Viscosity measurements<sup>16</sup> on PEEK in the presence of air in the temperature range of 350°C to 380°C showed an increase in viscosity with increasing dwell time, which was attributed to crosslinking. Chain extension may also be a possible cause for viscosity increase, but this is likely to be very limited because of the restricted mobility of the reactive groups. Degradation will result in a decrease in viscosity. Chain crosslinking or chain extension would only result in inhibiting crystallization. In our optical microscope studies the specimen has been heated between two glass plates with virtually no air gap. Melting and recrystallization over several cycles, melt time held to five minutes, resulted in reproducible spherulite size and growth rate although nucleation did not occur in the same positions after each melting. Also the PEEK resin between the microscope slides did not discolour on repeated melting except at the very edge. Therefore we believe that for this study significant degradation did not occur.

### Birefringence

The sign of the spherulite birefringence can be determined using a polarizing microscope or from V, light scattering<sup>13</sup>. A V, light scattering pattern of a PEEK sample, whose volume is completely filled with spherulites as observed in the polarizing microscope at room temperature, is given in Figure 4b. This scattering pattern is strongly oriented along the polarization direction, indicating that the difference between the radial and tangential polarizabilities is greater than the difference between either one of them and the effective polarizability of the surroundings of the spherulite. The surroundings of the spherulite consist of other spherulites since the whole volume is filled with them, and hence the polarizability of the surroundings will be the average of the radial and tangential polarizability. From this one can conclude that tangential polarizability is larger than the radial polarizability.

The spherulite birefringence sign was also determined, from room temperature to 320°C, using a polarizing microscope and a wave plate<sup>17</sup>. In the entire temperature range the spherulites were found to be negatively birefringent. The absolute value of birefringence was estimated using a Leitz tilting compensator to be approximately  $-0.02$ . The observation of negatively birefringent spherulites in PEEK is contrary to the previously published observation<sup>5</sup> in which PEEK spherulites were positively birefringent. Since the spherulite of the same material can be negatively or positively birefringent depending upon crystallization conditions, this difference in the birefringence sign between our and the previously published observation<sup>5</sup> needs further investigation.

The chain anisotropy can be calculated using the bond polarizabilities and the angles between different bonds<sup>18-20</sup>. Chain polarizability in three different directions is given by the following equations:

$$\alpha_a = \sum [(\alpha_1 - \alpha_2) \sin^2 \theta \cos^2 \phi + \alpha_2] \quad (2)$$

$$\alpha_b = \sum [(\alpha_1 - \alpha_2) \sin^2 \theta \sin^2 \phi + \alpha_2] \quad (3)$$

$$\alpha_c = \sum [(\alpha_1 - \alpha_2) \cos^2 \theta + \alpha_2] \quad (4)$$

where the summation is over the whole repeat unit,  $\theta$  is the angle which the bond makes with the  $c$ -axis, and  $\phi$  is the angle which the projection of the bond on the  $a$ - $b$  plane makes with the  $a$ -axis.  $\alpha_1$  and  $\alpha_2$  are the bond polarizabilities parallel and perpendicular to the bond, respectively. The bond polarizability values are listed in Table 1. The PEEK chain coordinates have been refined in our laboratory<sup>21</sup>. Using these refined coordinates the following values of polarizabilities were calculated.

$$\alpha_a = 3.38 \times 10^{-23} \text{ cm}^3$$

$$\alpha_b = 2.31 \times 10^{-23} \text{ cm}^3$$

$$\alpha_c = 4.02 \times 10^{-23} \text{ cm}^3$$

Polarizability of the chain and its refractive index,  $n$ , are related by the Lorenz-Lorentz equation:

$$\frac{(n^2 - 1)M}{(n^2 + 2)d} = \frac{4\pi}{3} \alpha N \quad (5)$$

**Table 1** Bond polarizabilities of various bonds<sup>18-20</sup>

Bond	$\alpha_1$ ( $10^{-25}$ cm <sup>3</sup> )	$\alpha_2$ ( $10^{-25}$ cm <sup>3</sup> )
C <sub>ar</sub> -C <sub>ar</sub>	22.5	4.8
C <sub>ar</sub> -C <sub>al</sub>	14.0	3.0
C-H	8.2	6.0
C-O	14.6	1.7
C=O	20.0	10.0

where  $N$  is Avogadro's number,  $d$  is the bulk density of the material and  $M$  is the molecular weight of the repeat unit. Using a PEEK crystalline density<sup>5</sup> of  $1.40$  g cm<sup>-3</sup> and the above values of chain polarizabilities in three different directions,  $n_a$ ,  $n_b$  and  $n_c$  were calculated to be 1.77, 1.48 and 1.97, respectively. Birefringence calculated using equation (5) is generally not in agreement with the observed value, and this is attributed to the presence of internal field effects. However, the birefringence in a spherulite and in a fibre was calculated using the above refractive indices. As will be noted in a later section, the  $b$  crystal axis is radial in the PEEK spherulite. Therefore the birefringence in the spherulite will be given by  $n_b - ((n_a + n_c)/2)$ , or  $n_{\text{spherulite}} = -0.39$ , which is about twenty times larger than the observed value. Such a difference in the observed and calculated birefringence has been attributed to imperfect crystalline orientation, the presence of amorphous regions, and form birefringence<sup>13</sup>.

The birefringence in the fibre will be given by  $n_c - ((n_a + n_b)/2)$  and for the above refractive indices its value is 0.34. Experimental measurement of birefringence on highly oriented PEEK fibres give birefringence values of up to 0.28. Because of the presence of less than perfect orientation in the fibre and the presence of amorphous regions, the true birefringence of the PEEK fibre would be higher than 0.28. This indicates that the calculated birefringence of PEEK fibre may be close to the true value.

#### Crystallinity and long period

Crystallinity was determined from wide-angle X-ray scattering (WAXS) using Ruland's method<sup>22-25</sup>. The main features of this method can be described by the following equations:

$$R(s_p^2) = \int_{s_0}^{s_p} s^2 I ds / \int_{s_0}^{s_p} s^2 I_{cr} ds \quad (6)$$

$$R(s_p^2) = 1/X_{cr} + (k/2X_{cr})s_p^2 \quad (7)$$

where  $s$  is  $2\sin\theta/\lambda$ , and  $\theta$  is half the scattering angle and  $\lambda$  the wavelength of radiation used,  $s_0$  and  $s_p$  represent the lower and upper limits of the scattering range,  $I$  and  $I_{cr}$  are the total and crystalline intensities respectively,  $X_{cr}$  is the degree of crystallinity and  $k$  is the disorder parameter. A typical plot of  $s^2 I$  versus  $s$  is given in Figure 7. An amorphous PEEK diffraction scan was fitted to the intensities between the crystalline peaks<sup>23</sup>, which is also shown in the shaded areas in Figure 7. From this curve  $R(s_p^2)$  was calculated for different values of  $s_p^2$ . A plot of  $R(s_p^2)$  as a function of  $s_p^2$  is given in Figure 8, which is approximately a straight line. From the slope and

intercept of this line the values of crystallinity and disorder parameters were obtained using equation (7).

Parameters obtained from WAXS and SAXS are listed in Table 2 for resin samples slow cooled from 400 and 420°C, and fast cooled from 400°C. From this table it is noted that, as expected, the fast cooled sample has both lower crystallinity and higher crystalline disorder compared with a slow cooled sample from the same melt temperature. For slow cooled samples, crystallization from a higher melt temperature gives rise to a slightly lower value of crystallinity and higher crystalline disorder. The crystallinity values of 36 to 43% are in the upper range of the reported<sup>5</sup> PEEK crystallinity values (0 to 45%). However it must be noted that the crystallinity as determined by Ruland's method<sup>22</sup> generally gives higher values than obtained from simple intensity ratios since the values from Ruland's method include disorder effects.

Approximate crystallite sizes were determined from the line breadth of the (211) reflection by Wilson's variance method<sup>26,27</sup>. The contribution to the line breadth from disorder was ignored and hence the crystal size reported in this paper represents the lower bound. The (211) reflection was chosen because it did not overlap other reflections. The size calculated for the sample slow cooled from 420°C was larger than the size calculated for the sample cooled from 400°C despite the higher disorder in

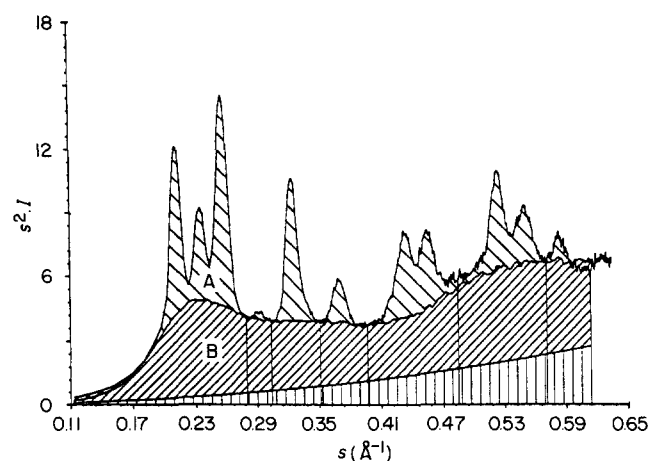


**Figure 7** Typical WAXS curve of PEEK, curve fitted using Pearson VII type function<sup>24,25</sup> (A) crystalline, and (B) amorphous

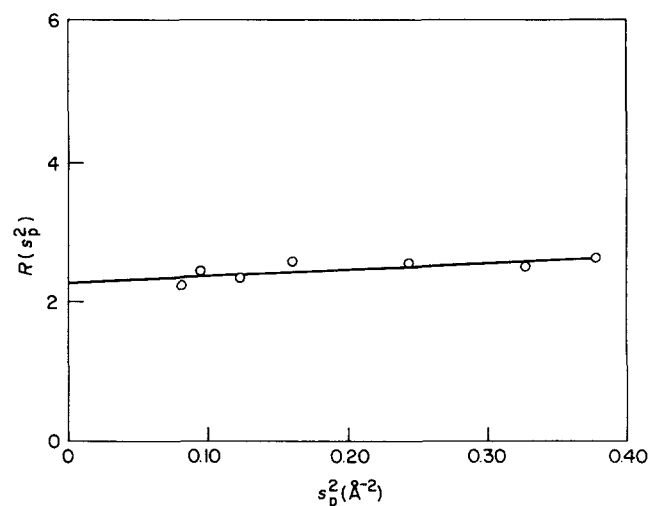


**Figure 8** Vonk<sup>23</sup> plot of  $R(s_p^2)$  versus  $s_p^2$

**Table 2** Parameters obtained from WAXS and SAXS

	Slow cooled from 400°C	Slow cooled from 420°C	Fast cooled from 400°C
Degree of crystallinity	0.43	0.38	0.36
Disorder parameter	0.61	2.85	1.75
Crystal size (Å)			
from (211)	50	63	41
(110)	110	123	110
(200)	79	92	72
Long period (Å)	160	170	—
Unit cell parameters (Å)			
<i>a</i> -axis	7.79	7.78	7.83
<i>b</i> -axis	5.91	5.90	5.92
<i>c</i> -axis	10.00	10.00	10.07

the sample from the higher temperature, which would tend to decrease the calculated size. The fast cooled sample shows an even smaller crystallite size. Approximate crystallite sizes were also calculated from the line broadening of the (110) and (200) reflections, which in turn were obtained by curve fitting the data. In the case of the (110) and (200) reflection the subtraction of the instrumental line broadening was done assuming gaussian profiles (the observed broadening is the sum of the squares of the specimen and instrumental broadening). The instrumental line profile was indeed gaussian; however the specimen profiles were best fitted with a Pearson type VII function. Again the sample slow cooled from 420°C shows larger crystallite sizes than the other two samples. In this analysis no significant differences between the fast and slow cooled samples from 400°C can be detected.

The unit cell parameters calculated from the positions of the reflections obtained during the curve fitting operation are also reported in *Table 2*. From these values it is noted that the fast cooled sample has larger values of *a* and *c* axes compared to the slow cooled sample. This larger unit cell for the crystals in the fast cooled sample is perhaps due to the chain packing disorder in the *a* and *c* axes directions.

While several differences were observed in the WAXS analysis, a greater range of process conditions will have to be investigated fully to understand the crystalline behaviour of this material.

#### Electron radiation damage

Different polymers are damaged in the electron beam to varying degrees<sup>28-31</sup>. In order to obtain useful information on the morphology of polymers using electron microscopy, it is important that the polymer not be exposed to such levels of electron radiation dose that the features of interest are destroyed or altered significantly. A systematic study was therefore undertaken<sup>31</sup> quantitatively to determine the dose required to damage different polymers to the point where the intensity of diffraction is reduced by a factor of 1/*e*. This dose level is generally termed as *D\** and its value for several polymers has previously been reported<sup>28</sup>. The *D\** value<sup>31</sup> for the (110) reflection of PEEK, at a dose rate of 10<sup>-3</sup> A cm<sup>-2</sup> is ~ 3 × 10<sup>-2</sup> C cm<sup>-2</sup>. This is about an order of magnitude greater than the *D\** value for polyethylene. The higher resistance of PEEK in the electron beam makes it relatively easier to study in the electron microscope.

#### Radial and growth direction

*Figure 9* shows an electron micrograph from a thin section microtomed from a specimen fast cooled from the melt at 400°C. In this *Figure*, as observed from selected area electron diffraction, regions marked A were amorphous and regions marked B were semicrystalline. The chatter produced due to microtoming is largely responsible for contrast in the A regions. The B regions are spherulites, which could not grow further due to fast cooling. In this specimen it was observed that a fraction of spherulites have grown to their fullest extent. From this it can be inferred that for complete crystallization from higher melt temperatures relatively slow cooling rates would be required. In the fast cooled sample row nucleation was also observed, as shown in *Figure 10*. Such nucleation has also been observed in isotactic polypropylene<sup>32</sup>.

Transmission electron micrographs of a section of a spherulite in two different directions in a sample slow cooled from the melt at 400°C are shown in *Figures 11a* and *b*. From photographs taken on a large number of

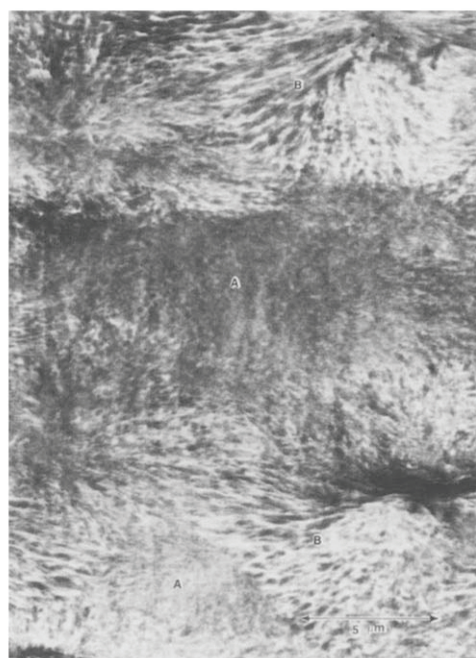


**Figure 9** Transmission electron micrograph (bright field) showing growth of spherulite. Regions marked 'A' are amorphous and regions marked 'B' are semicrystalline as determined from selected area electron diffraction

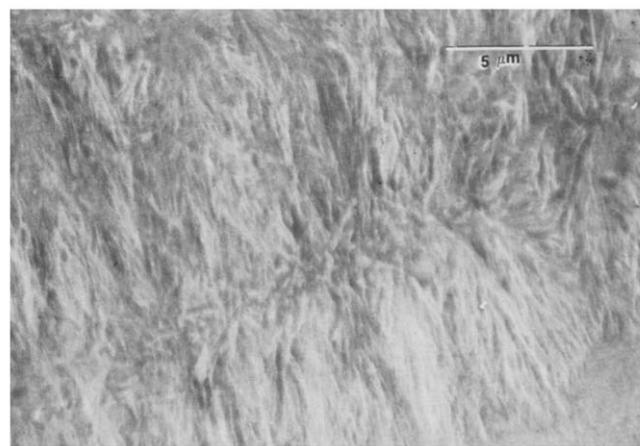


**Figure 10** Row nucleation in PEEK as observed in transmission electron microscopy

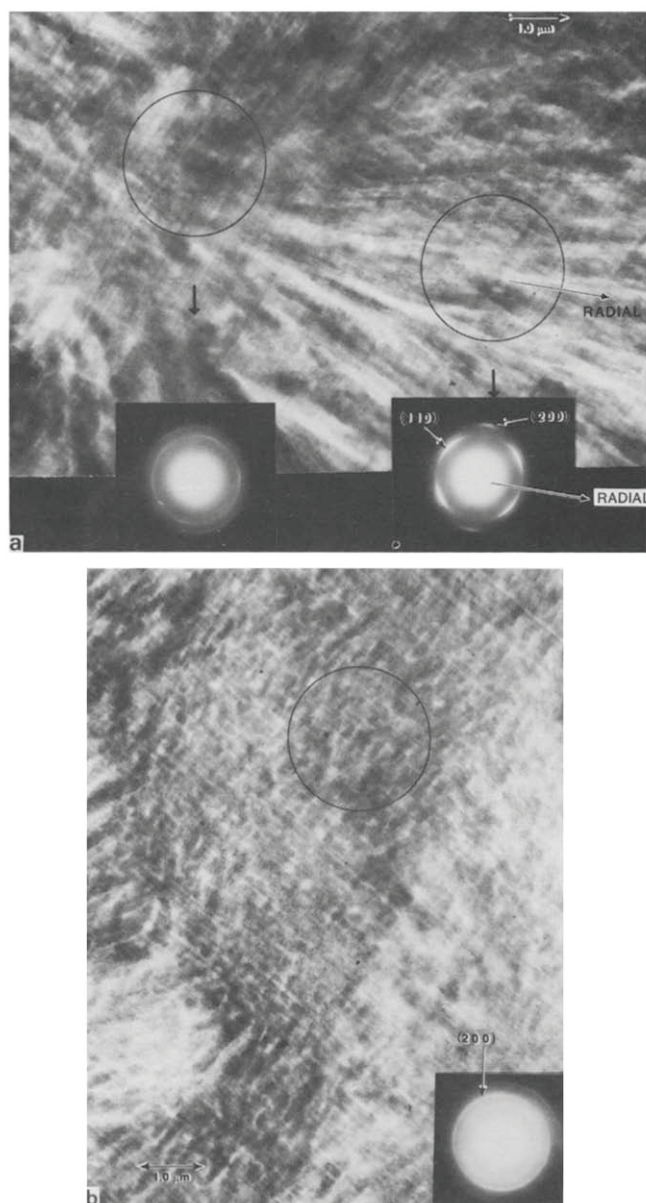


**Figure 11** Transmission electron micrographs (bright field) of spherulites seen (a) along radius, (b) perpendicular to radius, and selected area electron diffraction patterns from the areas indicated with arrows

sections it was ascertained that the section in *Figure 11a* is a diametrical section and the radial direction is in the plane of the paper. Selected area electron diffraction patterns taken from different regions are shown in *Figures 11a* and *b*; the corresponding regions are indicated by black circles. The two diffraction patterns in *Figure 11a* are similar except that the diffraction pattern from the centre of the spherulite is less oriented, as expected. The (110) reflection is the strongest in *Figure 11a* and is missing in *Figure 11b*. From the orientation of the diffraction pattern in *Figure 11a* it can be seen that the crystal unit cell *b* axis is radial and hence the *a* and *c* axes are tangential.

The growth direction of a spherulite is along its radius, and therefore one would expect that the preferred growth plane in PEEK spherulites would be a (010) plane. Information regarding the preferred growth plane can be obtained from dark field electron microscopy. A dark field electron micrograph using the (110) reflection is shown in *Figure 12*. Careful examination of the dark field electron micrographs (see the circled region in *Figure 12*) reveals

that the growth faces of the crystallites and the radial direction of the spherulite are not perpendicular to each other. From a large number of these crystals where the growth face was distinct, the angle between the radial direction and the growth face was measured to be  $55 \pm 8$  degrees. The calculated angle between the *b* axis and (110) plane is 52.7 degrees. This observation is suggestive of the fact that (110) is probably the preferred crystal growth plane. Following the dictates of the Bravais–Friedel law<sup>33</sup> the (110) plane was in fact assumed<sup>5</sup> to be the preferred growth plane in PEEK. Reported work on PEEK single crystals<sup>6</sup> also suggests (110) as the preferred growth plane.

One of the problems which one encounters in the electron microscopy of ultramicrotomed sections of polymers is the deformation introduced in the process of microtoming. Since we were using dark field micrographs obtained on ultramicrotomed sections to determine the preferred growth plane, the consideration of crystal orientation smearing due to ultramicrotoming was particularly important. Selected area electron diffraction on a large number of spherulites with different cutting directions indicated that the *b* crystal axis was always radial and was independent of microtoming direction, suggesting that no significant orientation smearing took place.

## CONCLUSIONS

Crystallization of PEEK from the melt is sensitive to the melt temperature, with significant differences observed in the nucleation density, but only small differences in other parameters such as degree of crystallinity, crystallite size, disorder and long period. Samples crystallized from higher melt temperature have a larger disorder parameters and larger crystals. The nucleation density decreases with higher melt temperature, thereby resulting in larger spherulites. Spherulite growth rate was faster at 300°C as compared to the growth rate at 320°C. PEEK crystallized from the melt was found to have negatively birefringent spherulites. However, since spherulites of the same material can be positively or negatively birefringent and since positively birefringent spherulites in PEEK have previously been reported, this aspect needs further work in order to resolve the question that there indeed are two different types of spherulites in PEEK. Calculated refractive indices of PEEK crystals along the three crystallographic axes *a*, *b* and *c* are, respectively, 1.77, 1.48 and 1.97. The *b* crystal axis is radial in the spherulites, and the crystals appear to have (110) as the preferred growth plane.

## ACKNOWLEDGEMENT

The atomic coordinates in the repeat unit were made available by Professor A. V. Fratini and the computer program for the calculation of chain polarizabilities was written by Dr P. T. Bapu of the University of Dayton. The authors are grateful for useful comments on the manuscript from Professor E. L. Thomas of the University of Massachusetts.

## REFERENCES

- 1 Dawson, P. C. and Blundell, D. J. *Polymer* 1980, **21**, 577
- 2 Rueda, D. R., Ania, F., Richardson, A., Ward, I. M. and Calleja, F. J. B. *Polymer* 1983, **24** (*Commun.*), 258

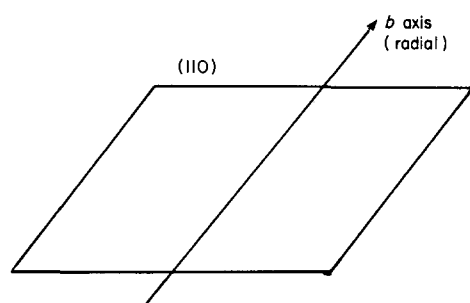
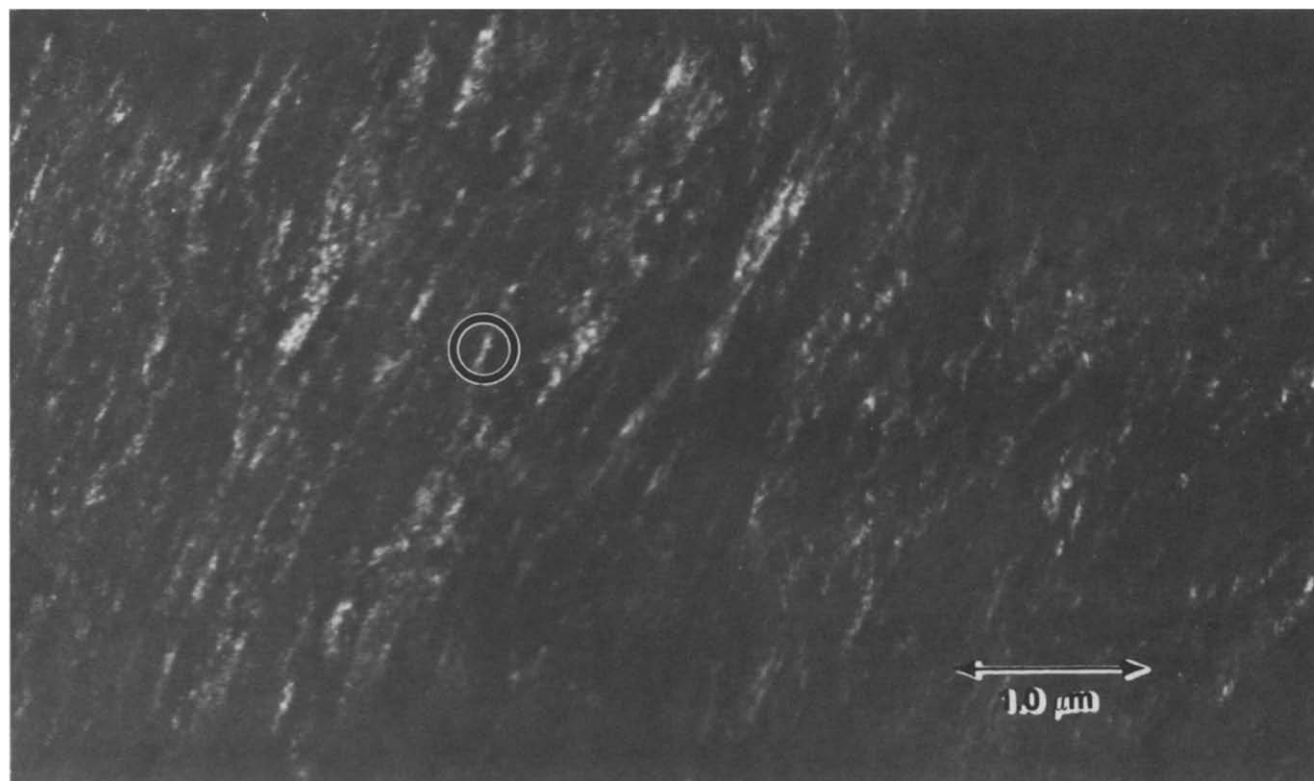


Figure 12 Transmission electron micrograph (dark field) using (110) plane and the schematic of crystal orientation. Scale bar – 1.0  $\mu\text{m}$

- 3 Hay, J. N., Kemmish, D. J., Langford, J. I. and Rae, A. I. M. *Polymer* 1984, **25** (*Commun.*), 175
- 4 Attwood, T. E., Dawson, P. C., Freeman, J. L., Hoy, L. R. J., Rose, J. B. and Staniland, P. A. *Polymer* 1981, **22**, 1096
- 5 Blundell, D. J. and Osborn, B. N. *Polymer* 1983, **24**, 953
- 6 Lovinger, A. J. and Davis, D. D. *Bull. Am. Phys. Soc.* 1985, **30**, 249, and the presentation at March 1985 APS meeting
- 7 Cebe, P., Hong, S. D., Chung, S. Y., Gupta, A. and Yavourian, A. in *Bull. Am. Phys. Soc.* 1985, **30**, 248, 488, 497
- 8 Bishop, M. T., Karasz, F. E., Russo, P. S. and Langley, K. H. *Macromolecules* 1985, **18**, 86
- 9 Wakelyn, N. T. *Polymer* 1984, **25** (*Commun.*), 307
- 10 Boon, J. and Magre, E. P. *Makromol. Chem.* 1969, **126**, 130
- 11 Hartness, J. T. and Kim, R. Y. *29th National SAMPE Symp.* 1984, **29**, 459 and 765
- 12 Tabar, R. J., Stein, R. S. and Long, M. J. *Polym. Sci., Polym. Phys. Edn.* 1982, **20**, 2041
- 13 Stein, R. S. and Rhodes, M. B. *J. Appl. Phys.* 1960, **31**, 1873; American Physical Society short course on 'Scattering Methods in Polymer Science' at Chicago (March 1979), coordinated by R. S. Stein
- 14 Wunderlich, B. 'Macromolecular Physics, Vol. II—Crystal Nucleation, Growth, Annealing', Academic Press, 1976, p. 52, and references cited on p. 53
- 15 Johnson, R. N., Fahrnam, A. G., Clendinning, R. A., Hale, W. F. and Merrian, C. F. *J. Polym. Sci., Polym. Chem. Edn.* 1967, **5**, 2375
- 16 Nicholls, D. J. Personal communication
- 17 Chamot, E. M. and Mason, C. W. 'Handbook of Chemical Microscopy', Vol. I, John Wiley and Sons, 1958, p. 300
- 18 Bunn, C. W. 'Chemical Crystallography', Oxford University Press, London, 1961, p. 312
- 19 Furukawa, J., Yamashita, S., Kotani, T. and Kawashima, M. *J. Appl. Polym. Sci.* 1969, **13**, 2527
- 20 Roche, E. J., Stein, R. S. and Thomas, E. L. *J. Polym. Sci., Polym. Phys. Edn.* 1980, **18**, 1145
- 21 Fratini, A., Cross, E., Whitaker, R. and Adams, W. W., submitted to *Polymer*
- 22 Ruland, W. *Acta Crystallogr.* 1961, **14**, 1180
- 23 Vonk, C. G. *J. Appl. Crystallogr.* 1973, **6**, 148
- 24 Anderson, D. P. AFWAL-TR-85-4079, WPAFB, Ohio, 1985
- 25 Hall, M. M., Jr., Veeraraghavan, V. G., Rubin, H. and Winchell, P. G. *J. Appl. Crystallogr.* 1977, **10**, 66
- 26 Wilson, A. J. C. *Proc. Physical Soc., London* 1962, **80**, 286
- 27 Pitts, E. and Willets, F. W. *Acta Crystallogr.* 1961, **14**, 1302
- 28 Minter, J. R. *Ph.D. Thesis*, University of Massachusetts, Amherst, p. 104 (1982)
- 29 Thomas, E. L. and Ast, D. G. *Polymer* 1974, **15**, 37
- 30 Grubb, D. T. and Groves, G. W. *Phil. Mag.* 1971, **24**, 815
- 31 Kumar, S., Krause, S. J. and Adams, W. W. *Proc. Electr. Microscopy Soc. Am.* 1985, **43**, 84
- 32 Maxwell, B. *J. Polym. Sci.* 1965, **C9**, 43
- 33 Wunderlich, B. 'Macromolecular Physics, Vol. I—Crystal Structure, Morphology, Defects', Academic Press, 1973, p. 182